

***Generation of anisotropic-smoothness
regularization filters for EIT***

Borsic, A. and Lionheart, W.R.B. and McLeod, C.N.

2002

MIMS EPrint: **2006.243**

Manchester Institute for Mathematical Sciences
School of Mathematics

The University of Manchester

Reports available from: <http://eprints.maths.manchester.ac.uk/>

And by contacting: The MIMS Secretary
School of Mathematics
The University of Manchester
Manchester, M13 9PL, UK

ISSN 1749-9097

Generation of Anisotropic-Smoothness Regularization Filters for EIT

Andrea Borsic, William R. B. Lionheart, and Christopher N. McLeod*

Abstract—In the inverse conductivity problem, as in any ill-posed inverse problem, regularization techniques are necessary in order to stabilize inversion. A common way to implement regularization in electrical impedance tomography is to use Tikhonov regularization. The inverse problem is formulated as a minimization of two terms: the mismatch of the measurements against the model, and the regularization functional. Most commonly, differential operators are used as regularization functionals, leading to smooth solutions. Whenever the imaged region presents discontinuities in the conductivity distribution, such as interorgan boundaries, the smoothness prior is not consistent with the actual situation. In these cases, the reconstruction is enhanced by relaxing the smoothness constraints in the direction normal to the discontinuity. In this paper, we derive a method for generating Gaussian anisotropic regularization filters. The filters are generated on the basis of the prior structural information, allowing a better reconstruction of conductivity profiles matching these priors. When incorporating prior information into a reconstruction algorithm, the risk is of biasing the inverse solutions toward the assumed distributions. Simulations show that, with a careful selection of the regularization parameters, the reconstruction algorithm is still able to detect conductivities patterns that violate the prior information. A generalized singular-value decomposition analysis of the effects of the anisotropic filters on regularization is presented in the last sections of the paper.

Index Terms—Anisotropic smoothing, electrical impedance tomography, GSVD, prior information, regularization.

I. INTRODUCTION

ELECTRICAL impedance tomography involves reconstructing the conductivity of an object from current and voltage measurements on the boundary. Usually, electrodes are applied to the object and known currents are passed through some of them; the resulting voltages are measured on the electrodes. Reconstruction algorithms make use of a forward model: simulated measurements are matched to the real ones by acting on the discretized conductivity of the model; the reconstructed conductivity is the solution of the least-squares problem

$$\mathbf{s}_{\text{rec}} = \operatorname{argmin} \|\mathbf{h}(\mathbf{s}) - \mathbf{z}\|^2 \quad (1)$$

where \mathbf{z} is the vector of measured voltages, \mathbf{s} is the discrete conductivity, and \mathbf{h} is the nonlinear forward operator from model space to measurements space.

The reconstruction problem is ill conditioned and regularization techniques are necessary in order to stabilize the process. Commonly, (1) is solved using the Tikhonov regularization, formulating the reconstruction as

$$\mathbf{s}_{\text{rec}} = \operatorname{argmin} \{\|\mathbf{h}(\mathbf{s}) - \mathbf{z}\|^2 + \alpha^2 F(\mathbf{s})\} \quad (2)$$

where $F(\mathbf{s}) \geq 0$ is the regularization functional and α is the regularization parameter. The conductivity being discrete, the regularization functional is usually expressed as $F(\mathbf{s}) = \|\mathbf{L}\mathbf{s}\|^2$, where \mathbf{L} is the regularization matrix. The reconstruction is, therefore, formulated as

$$\mathbf{s}_{\text{rec}} = \operatorname{argmin} \{\|\mathbf{h}(\mathbf{s}) - \mathbf{z}\|^2 + \alpha^2 \|\mathbf{L}\mathbf{s}\|^2\}. \quad (3)$$

The role of the regularization functional is to penalize solutions that according to some prior knowledge are unlikely. A classic choice for the matrix \mathbf{L} is suggested by the identity matrix, a similar choice is made by the NOSER algorithm [1] which uses a positive diagonal matrix. Matrices that approximate first- and second-order differential operators have also been commonly used in electrical impedance tomography (EIT) over the last decade [2]. All these regularization methods achieve the stability of the inversion by penalizing sudden variations in the conductivity; the cost is that the reconstruction is rendered incapable of describing sharp variations.

There are of course situations of practical interest where the actual conductivity presents sudden variations. In the literature, two different approaches have been proposed for dealing with those situations. The first approach seeks solutions with the least total variation [3] or uses the total variation as a regularization functional [4], allowing the presence of step changes in the reconstructed images. This approach is particularly suitable for reconstructing piece-wise constant conductivities, although it might lead to staircase effects in the presence of conductivity gradients.

The second approach is that of incorporating structural prior information into the reconstruction process to estimate the unknown conductivity more closely [5]–[9]. By this means, it is possible to enhance the sharpness of the images when the prior information is matched by the actual experiment, as shown by Kaipio *et al.* [10].

The approach followed in [10] is to use anisotropic smoothness constraints in the regularization. The smoothness constraints are relaxed along the direction of the expected

Manuscript received August 1, 2001; revised March 3, 2002. Asterisk indicates corresponding author.

A. Borsic is with the School of Engineering, Oxford Brookes University, OX3 0BP Oxford, U.K.

W. R. B. Lionheart is with the Department of Mathematics, UMIST, M60 1QD Manchester, U.K.

*C. N. McLeod is with the School of Engineering, Oxford Brookes University, Tonge Bldg. T6.06, OX3 0BP Oxford, U.K. (e-mail: cmcleod@brookes.ac.uk)

Publisher Item Identifier 10.1109/TMI.2002.800611.

changes, allowing faster transitions in this direction while preserving the necessary smoothness tangentially. The study proposes a way of constructing the filters for a piece-wise linear two-dimensional (2-D) finite-element method (FEM) forward model. The conductivity being linear, it is possible to express the first partial derivatives of each element as functions of the nodal values of \mathbf{s} . The reconstruction then penalizes them differently, according to the local direction of the expected changes.

In this paper, we present a method for constructing Gaussian anisotropic filters for a piece-wise constant 2-D FEM forward model. As the spatial derivatives are not readily available, the filters express their directional properties by weighting appropriately the conductivity values of neighboring elements. The approach is introduced first by analyzing the traditional forms of regularization, then extending Gaussian isotropic filtering to the anisotropic case.

II. STANDARD REGULARIZATION

An insight on the ill conditioning of the reconstruction problem and on traditional regularization techniques is gained by linearizing (1) about a point \mathbf{s}_0

$$\delta \mathbf{s}_{\text{rec}} = \operatorname{argmin} \|J\delta \mathbf{s} - (\mathbf{z} - h(\mathbf{s}_0))\|^2 \quad (4)$$

and by analyzing the singular-value decomposition (SVD) of the Jacobian J of the forward operator. The matrix $J \in \mathbb{R}^{m \times n}$ (m is the number of observations, and n is the number of elements in which the conductivity has been discretized) is decomposed as

$$J = U\Sigma V^T \quad (5)$$

where U and V are $m \times m$ and $n \times n$ orthonormal matrices and $\Sigma = \operatorname{diag}(\lambda_1, \dots, \lambda_n)$ with $\lambda_1 \geq \dots \geq \lambda_n \geq 0$. Given the decomposition, the mapping $J\delta \mathbf{s}$ of a change in the conductivity $\delta \mathbf{s}$ can be expressed as

$$J\delta \mathbf{s} = \sum_{i=1}^n \mathbf{u}_i \lambda_i (\mathbf{v}_i^T \delta \mathbf{s}). \quad (6)$$

The ill posedness of the problem is shown by the singular values λ_i rapidly decaying to zero: there are certain changes in \mathbf{s} parallel to the higher singular vectors (SVs) \mathbf{v}_i that are strongly attenuated and would become unobservable in the presence of noise.

When inverting the conductivity, assuming that J has full rank, solutions of (4) are expressed as

$$\delta \mathbf{s}_{\text{rec}} = \sum_{i=1}^n \frac{(\mathbf{u}_i^T \delta \mathbf{z})}{\lambda_i} \mathbf{v}_i. \quad (7)$$

Terms with higher values of i , for which observations are poor, are strongly amplified by the factor $1/\lambda_i$, leading to a solution that is dominated by noise.

The aim of regularization is, therefore, to dampen the contribution of the higher SVs to the reconstructed image. This is achieved explicitly by the truncated SVD technique stopping the summation of (7) at an index $k < n$ for which the observations are not exceeded by the noise level.

A similar filtering effect is achieved implicitly, at a minor computational expense, by using the identity matrix in the regularization term or by using the NOSER algorithm, for which the regularized solutions of (4) are expressed as

$$\delta \mathbf{s}_{\text{rec}} = \sum_{i=1}^n \frac{\lambda_i}{\lambda_i^2 + \alpha^2 l_i} (\mathbf{u}_i^T \delta \mathbf{z}) \mathbf{v}_i \quad (8)$$

where l_i are the diagonal elements of L . The regularization prevents the multiplicative term from diverging for $\lambda_i \rightarrow 0$.

Similarly, the effect of regularization matrices that are discrete approximations of first- and second-order differential operators can be understood in terms of SVD decomposition by considering the fact that higher SVs \mathbf{v}_i tend to be more and more oscillatory, therefore constraining the image to be smooth rejects their contribution.

All the standard techniques, therefore, stabilize the inversion by limiting the unreliable contribution of the higher SVs to the reconstructed images.

III. STATISTICAL INTERPRETATION OF L

A similar regularization approach is suggested by the statistical interpretation of the reconstruction [11]. In this case, the discretized conductivity \mathbf{s} is assumed to be a random variable and the observations \mathbf{z} to be contaminated by the random noise \mathbf{n}

$$\mathbf{z} = h(\mathbf{s}) + \mathbf{n}. \quad (9)$$

Assuming also that \mathbf{s} is a Gaussian variable with mean \mathbf{m}_s and covariance matrix C_s and that \mathbf{n} has zero mean and covariance matrix C_n , the posterior probability density for the vector \mathbf{s} given the observation \mathbf{z} is

$$p_s(\mathbf{s} | \mathbf{z}) = \frac{p_z(\mathbf{z} | \mathbf{s})p_s(\mathbf{s})}{p_z(\mathbf{z})}. \quad (10)$$

Where subscripts indicate which probability density p is used. Additionally, recalling (9)

$$p_z(\mathbf{z} | \mathbf{s}) = p_n(\mathbf{z} - h(\mathbf{s}) | \mathbf{s}). \quad (11)$$

If \mathbf{s} and \mathbf{n} are statistically independent

$$p_z(\mathbf{z} | \mathbf{s}) = p_n(\mathbf{z} - h(\mathbf{s})). \quad (12)$$

Given that $p_z(\mathbf{z})$ is a constant since \mathbf{z} is fixed, and using (10) and (12)

$$p_s(\mathbf{s} | \mathbf{z}) \propto \exp \left\{ -\frac{1}{2}(\mathbf{z} - h(\mathbf{s}))^T C_n^{-1}(\mathbf{z} - h(\mathbf{s})) \right\} \cdot \exp \left\{ -\frac{1}{2}(\mathbf{s} - \mathbf{m}_s)^T C_s^{-1}(\mathbf{s} - \mathbf{m}_s) \right\}. \quad (13)$$

If \mathbf{s} is now estimated with the *maximum a posteriori* (MAP) criterion, the maximum of $p_s(\mathbf{s} | \mathbf{z})$ is sought, which is equivalent to minimizing the argument of the exponentials in (13)

$$\mathbf{s}_{\text{MAP}} = \operatorname{argmin} \left\{ (\mathbf{z} - h(\mathbf{s}))^T C_n^{-1}(\mathbf{z} - h(\mathbf{s})) + (\mathbf{s} - \mathbf{m}_s)^T C_s^{-1}(\mathbf{s} - \mathbf{m}_s) \right\}. \quad (14)$$

Formally, the Tikhonov solution of the inverse problem (3) is identical to the MAP approach when $C_n^{-1} = I$, $L^T L \propto C_s^{-1}$ and \mathbf{m}_s is a prior estimate of \mathbf{s} . This connects the choice of L to the statistical information on \mathbf{s} .

The properties of C_s reflect the prior knowledge of the system under measurement. The diagonal elements of the matrix represent the variance of each element in the image, the off-diagonal elements of the matrix are a function of the correlation r between elements of the image $C_{s_{ij}} = r\sqrt{C_{s_{ii}}C_{s_{jj}}}$. It is, therefore, possible to envisage the possibility of constructing C_s^{-1} on the basis of the structural knowledge of the system under measurement, and of using a regularization matrix L such that $L^T L \propto C_s^{-1}$.

IV. ISOTROPIC GAUSSIAN SMOOTHING

The latter approach, $L^T L \propto C_s^{-1}$, has been considered by Adler *et al.* [12], even though the authors finally assumed only the implicit information that a limited resolution is achieved by EIT. They, therefore, used a covariance matrix that allowed some correlation between neighboring image elements. In this case, the inversion of the covariance matrix is ill posed and, thus, numerically unstable. Observing that the covariance matrix has the structure of a lowpass filter, the solution they proposed is to use a Gaussian highpass filter to represent its inverse. For the 2-D case, the frequency response of the filter with a spatial frequency of ω_o is

$$G(\tau, \nu) = 1 - \exp(-\omega_o(\tau^2 + \nu^2)) \quad (15)$$

with the following convolution kernel:

$$g(x, y) = \delta(x, y) - \frac{\pi}{\omega_o^2} \exp\left(-\frac{\pi^2}{\omega_o^2}(x^2 + y^2)\right). \quad (16)$$

A regularization matrix L that approximates the filter can be found by expressing the filtered value $\hat{\sigma}$ of the continuous conductivity σ at the mid-point coordinates x_i, y_i of the i th element of the image

$$\hat{\sigma}(x_i, y_i) = g(x, y) * \sigma(x, y)|_{x=x_i, y=y_i} \quad (17)$$

and assigning the value at the mid-point to the discrete conductivity

$$\hat{\mathbf{s}}_i = \int g(x_i - x, y_i - y) \sigma(x, y) dx dy. \quad (18)$$

The integration can be carried out on the single elements E_j , after bringing the piece-wise constant conductivity out of the integration

$$\hat{\mathbf{s}}_i = \sum_j \mathbf{s}_j \int_{E_j} g(x_i - x, y_i - y) dx dy \quad (19)$$

the filtered conductivity can be expressed as $\hat{\mathbf{s}} = L \mathbf{s}$ with the following definition for L :

$$L_{ij} = \int_{E_j} g(x_i - x, y_i - y) dx dy. \quad (20)$$

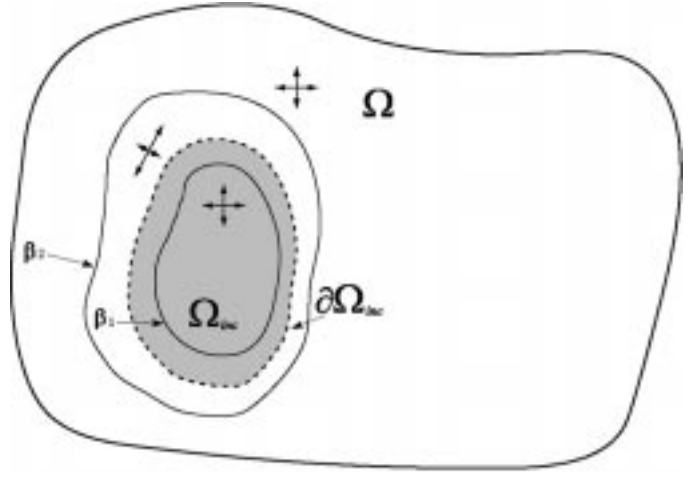


Fig. 1. An object Ω has an inclusion Ω_{inc} with a different conductivity (gray area). The contour of the inclusion is bounded by β_1 and β_2 and is expected to follow approximately the bounding profiles. In order to exploit the structural information, the smoothing filter weights (represented by crosses) should be anisotropic in the region bounded by the two β curves, allowing for a faster variation of the conductivity in the direction of the expected changes.

V. ANISOTROPIC GAUSSIAN SMOOTHING

The statistical interpretation of the matrix L sets the basis for incorporation of prior structural information into regularization. In their study, Adler *et al.*, however, did not assume this information and used an isotropic Gaussian filter in order to mimic C_s^{-1} . Nevertheless, their proposed method inspired the use of an anisotropic Gaussian kernel that we adopt in this study for exploiting the anatomical priors, which are, in the medical imaging context, the equivalent of the structural information.

We now consider the problem for which we propose a method by examining the situation presented in Fig. 1. Assume that a body Ω has an inclusion Ω_{inc} that presents a different conductivity from the surrounding body. The shape of the inclusion is not precisely known, but it is bounded by β_2 and β_1 . The boundary $\partial\Omega_{\text{inc}}$ of the object is assumed to follow approximately the bounding curves. An organ expanding and contracting during its physiological activity could be an example of the depicted situation.

The region enclosed between the two bounding curves β , which we label Ω_{change} , is where the expected conductivity discontinuity will occur. The objective is to relax the smoothing constraints in the region Ω_{change} along the direction normal to the line of changes, that has yet to be defined. The tangential smoothing can be maintained, expecting the changes to be orthogonal to that direction.

We, therefore, propose to use the anisotropic Gaussian kernel that is obtained by transforming (16)

$$g(n, t) = \delta(n, t) - \frac{\pi}{\omega_n \omega_t} \exp\left(-\pi^2 \left(\frac{n^2}{\omega_n^2} + \frac{t^2}{\omega_t^2}\right)\right) \quad (21)$$

where n and t are the tangential and normal directions of the expected changes in the conductivity. Such a kernel would separate control of the smoothing along n and t by varying the parameters ω_n and ω_t . From a statistical point of view, this is equivalent to assuming that the image elements are less correlated in the direction of the expected changes.

Theoretically, the use of such a filter is straightforward; in practice the problem is to find a way of calculating the system of coordinates (n, t) given the geometry of the domains. The normal and tangential directions need to be defined somehow in the region Ω_{change} , in order to make the use of the Gaussian anisotropic kernel possible.

VI. FINDING NORMAL AND TANGENTIAL COORDINATES

The problem of finding the normal and tangential coordinates can be solved naturally with a system of harmonic coordinates. The intention is to find a system of coordinates where

$$\hat{n} \perp \beta_1, \quad \text{on } \beta_1 \quad (22)$$

$$\hat{n} \perp \beta_2, \quad \text{on } \beta_2 \quad (23)$$

$$\hat{t} \perp \hat{n}, \quad \text{in } \Omega_{\text{change}}. \quad (24)$$

The solution we propose is to find (\hat{n}, \hat{t}) satisfying (22)–(24) by solving a partial differential equation (PDE).

Solving $\nabla^2 n = 0$ over Ω_{change} with the following Dirichlet boundary conditions:

$$\begin{aligned} n = 1, & \quad \text{on } \beta_1 \\ n = 0, & \quad \text{on } \beta_2 \end{aligned} \quad (25)$$

gives a solution n defined over all the domain Ω_{change} that can be regarded as one of the coordinates of the system (n, t) . Points with $n = 0$ will lie on β_2 , points with $n = 1$ will lie on β_1 . The vector $\hat{n} \equiv \nabla n$ is orthogonal to β_1 for $n = 1$ and orthogonal to β_2 for $n = 0$. Therefore, \hat{n} satisfies (22) and (23). Now assume a crack in the domain Ω_{change} as illustrated in Fig. 2, and that $\nabla^2 t = 0$ is solved over Ω_{change} with Dirichlet boundary conditions

$$\begin{aligned} t = 0, & \quad \text{on one side of the crack.} \\ t = 1, & \quad \text{on the other side of the crack.} \end{aligned} \quad (26)$$

and Neumann conditions ($\partial t / \partial \hat{n} = 0$) on β_1 and β_2 . The solutions n and t will form a system of harmonic coordinates. The level sets of t are distributed radially on the domain Ω_{change} , giving a vector $\hat{t} \equiv \nabla t$ that is orthogonal to \hat{n} on it, satisfying (24). The coordinate change $(x, y) \rightarrow (n, t)$ maps the cracked domain Ω_{change} to the rectangle $[0, 1] \times [0, 1]$ in \mathbb{R}^2 . The coordinates (n, t) can, therefore, be used to carrying out the integration of the kernel (21) producing an anisotropic weighting matrix L .

VII. COMMENTS ON CALCULATION OF L

The idea of solving a PDE for the calculation of (n, t) was based on the opportunity of relying mostly on the forward solver for the task. In EIT, the forward algorithm solves

$$\nabla \cdot \sigma \nabla u = 0 \quad (27)$$

where u is the electric potential. It is sufficient to set σ to a constant value in (27) order to enable the forward solver to solve the Laplace equation. In order to apply Dirichlet boundary con-

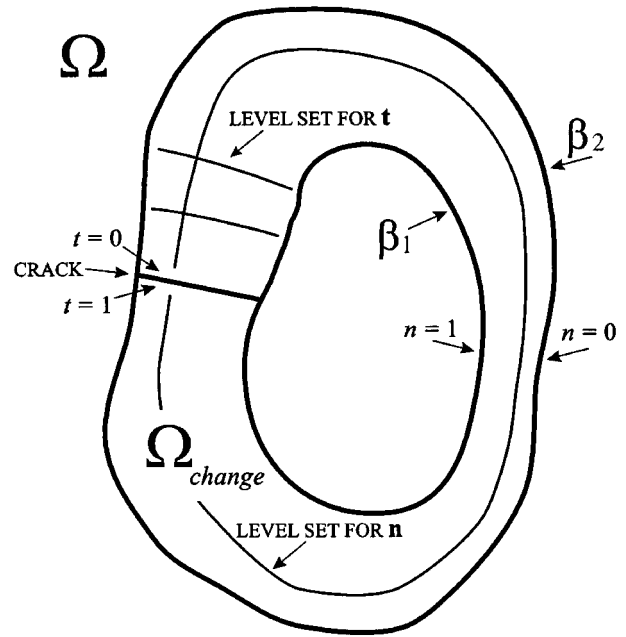


Fig. 2. Calculation of the normal and tangential coordinates solving the Laplace equation over the domain Ω_{change} with opportune boundary conditions. The solutions n and t form a system of harmonic coordinates (n, t) that maps the cracked domain Ω_{change} to a rectangle.

ditions, however, the solver needs to be slightly modified; in fact, Neumann or constrained Robin conditions are applied in EIT depending on which electrode model is implemented [13].

An algorithm for the calculation of (n, t) has been developed in the MATLAB environment and integrated with the routines currently in use for the forward solution. The algorithm presupposes that a FEM mesh matching the external and internal boundaries of the object to be imaged has been produced. The user describes the structural information by selecting on the screen the nodes on β_1, β_2 . Given the two spatial frequencies ω_n and ω_t the algorithm computes the transformation of the domain Ω_{change} and calculates the anisotropic regularization matrix L .

For each finite-element E_i belonging to the domain Ω_{change} , the corresponding row of L_i is calculated by integrating (21), while for the rest of the elements the isotropic kernel (16) is used.

VIII. SIMULATIONS

In this section, we compare reconstructions using prior information, in the form of anisotropic smoothing, and traditional reconstructions using Gaussian isotropic smoothing. A simple experiment involving a square inclusion embedded in a round object was set up. The experiment has no physiological meaning but its validity is general. The numerical simulations allowed us to compare the two methods, and to present a generalized SVD (GSVD) analysis of the effect of prior information on the regularization.

A. Setup of the Experiment

The numerical experiment was set up as illustrated in Fig. 3. An outer round object with a diameter of 30 cm is expected

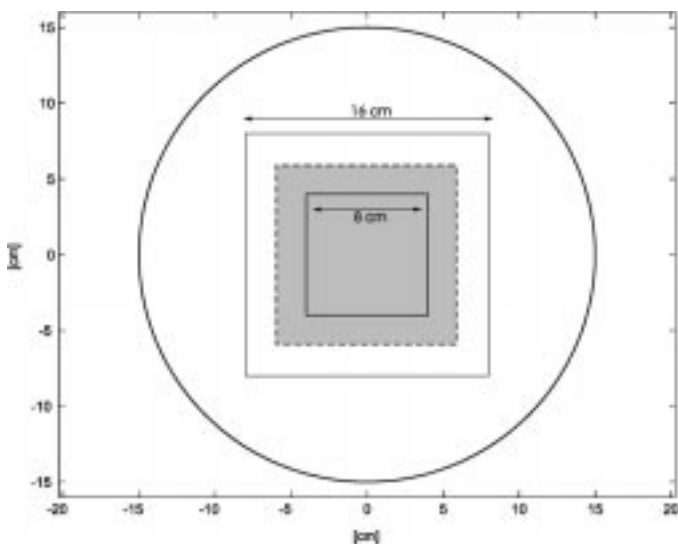


Fig. 3. Setup of the simulated experiment: round object with a square inclusion, definition of the domains and dimensions in centimeters.

to contain a square-shaped inclusion with a different conductivity. The dimensions of the inclusion can vary, the side of the anomaly can range from 8 cm to 16 cm.

A mesh of 798 triangular elements, shown in Fig. 4, was used for the inverse computations. The mesh matches the internal boundaries β_1 and β_2 in order to allow the calculation of (n, t) with the PDE method. The forward solver uses a finer mesh for calculating the electric potential, attaining higher accuracy in the forward solutions. The finer mesh was obtained from an adaptive refinement of the first mesh, resulting in 6346 elements. The mesh was used also for the generation of the test conductivity profiles of the simulations. The inclusions of the test profiles were generated not coincide with the discretization of the coarse mesh, as this would be not representative of a real situation. The disposition of the electrodes resembles the setup of the OXBACT III [14] adaptive current tomograph: 32 current electrodes, each one capable of injecting a current, are interleaved with another 32 electrodes, used to measure the electric potential, resulting in a total of 64 electrodes equispaced around the object.

B. Reconstructions

A first test conductivity profile matching the expected structure was used to compare the reconstructions with and without prior information. In the simulations, the conductivity of the surrounding circular object was set to $1 \Omega^{-1}\text{m}^{-1}$, and an 11-cm square inclusion, with conductivity $0.7 \Omega^{-1}\text{m}^{-1}$, was generated, as shown in Fig. 5(a).

For the reconstructions, trigonometric current patterns were used and the resulting measurements were calculated with a forward solver implementing the complete electrode model. A Gaussian white noise with zero mean and a standard deviation of 0.1% of the voltage range was added to the measurements to simulate instrument noise [15]. The reconstruction (3) is solved iteratively, starting from a homogeneous conductivity that best fits the data. The first four steps of the algorithm were performed. In Fig. 5(b) and (c), respectively, the isotropic and

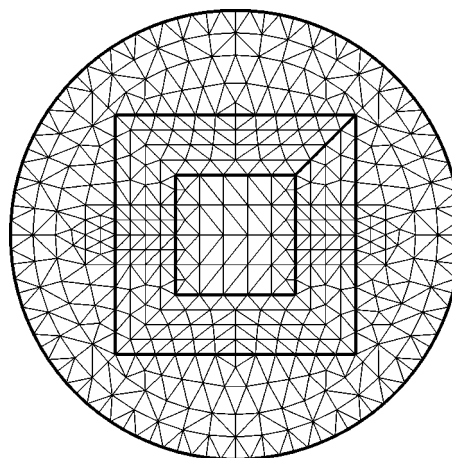


Fig. 4. Generated mesh, boundaries, and crack are shown in thick line.

anisotropic reconstructed conductivities are shown. Several values of the ratio ω_n/ω_t were used; a high ratio produces an image conforming strongly with the prior information, while a low ratio is close to conventional Gaussian smoothing. An anisotropy of 2.5 was found to be a good compromise for these experiments. As expected the isotropic solution smooths the lateral discontinuities of the square inclusion and rounds off the corners. The anisotropic solution, incorporating the prior information, estimates the square shape of the detected object more accurately.

In Fig. 6(a) and (b), cross sections of the true and reconstructed conductivities are shown for an easier quantitative comparison. Fig. 6(a) illustrates a cross section along the x axis. The anisotropic solution follows the sharp transitions and settles closer to the correct value in the center of the object than the isotropic one. The effect is more evident in Fig. 6(b), where the cross section is cut on the 45° diagonal, crossing the corners of the inclusion. The discontinuity of the corners is even more difficult to describe for the isotropic smoothing, resulting in a larger difference in the two reconstructions.

C. Incorrect Priors

The risk in using prior information in the reconstruction process is to bias the solution toward the assumed distribution, and to miss inclusions that do not respect the prior assumptions.

In this section, are presented reconstructions comparing the two methods in the case where the priors are incorrect. Fig. 7(a) shows the test conductivity to be reconstructed. The inclusion is a rectangular object with the lateral edges orthogonal to the direction assumed for the conductivity changes in Ω_{change} . The object, therefore, violates the prior information assumed by the regularization. The conductivity values for this test are again $1 \Omega^{-1}\text{m}^{-1}$ for the embedding object and $0.7 \Omega^{-1}\text{m}^{-1}$ for the inclusion. In Fig. 7(b) and (c), the isotropic and anisotropic reconstructions are shown. Both reconstructions were performed with the same parameters $(\alpha, \omega_n, \omega_t)$ as the ones used for the results of Fig. 5, and the same level of noise. The anisotropic solution detects the anomaly and locates it correctly. Some fake responses are, however, triggered in the Ω_{change} region, resulting in a poorer performance when compared with the isotropic reconstruction.

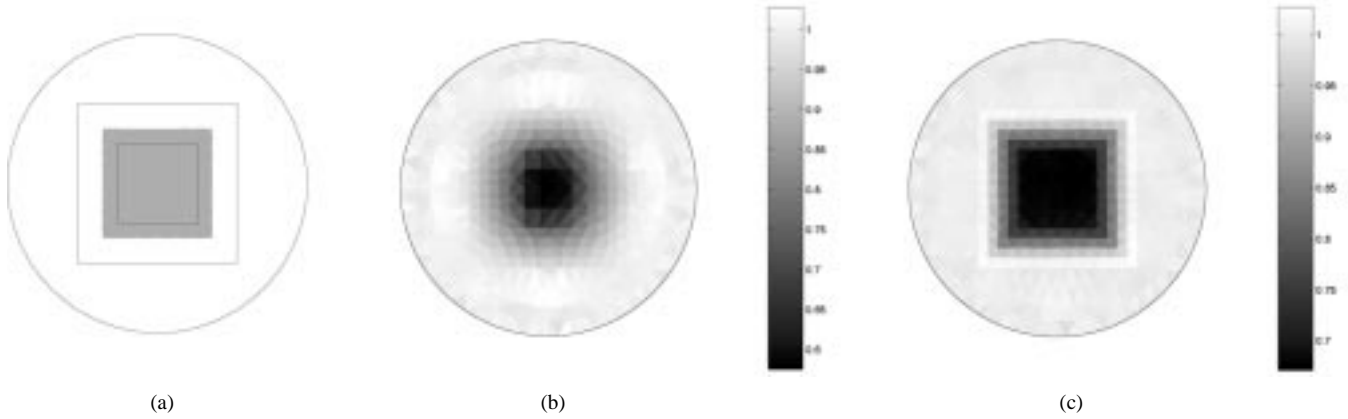


Fig. 5. Comparisons of isotropic and anisotropic priors. (a) Test conductivity profile. (b) Reconstruction with Gaussian isotropic smoothing of the 10-cm square inclusion. (c) Reconstruction using a Gaussian anisotropic filter.

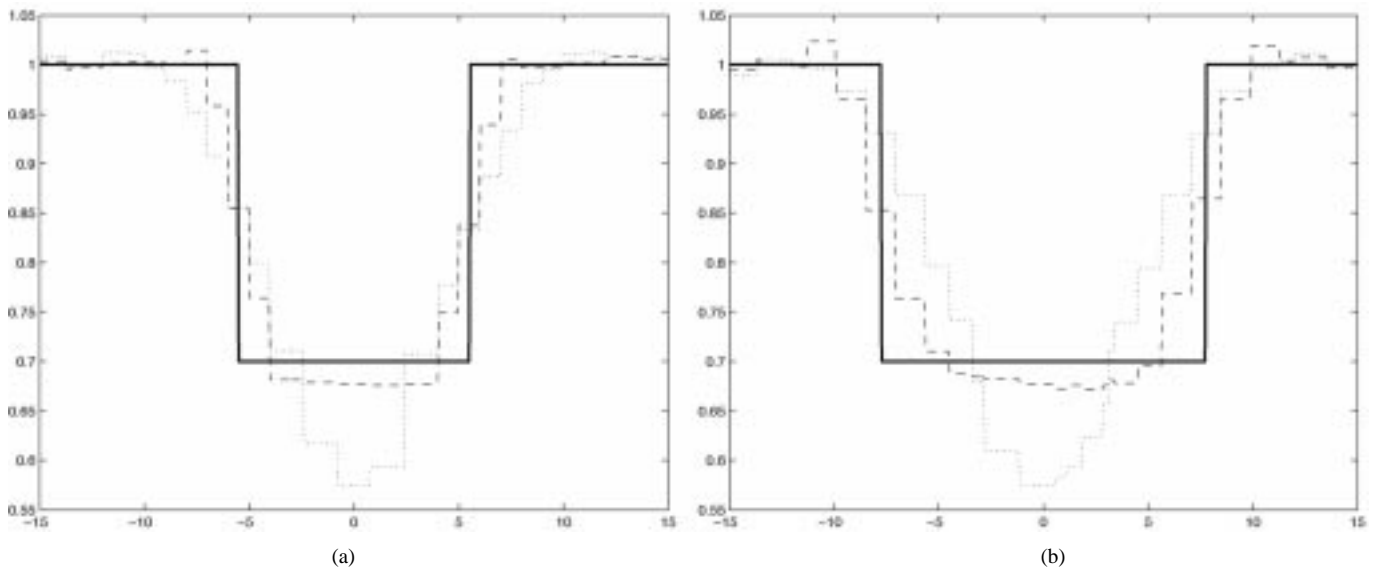


Fig. 6. Cross sections of the reconstructions. The thick line represents the true conductivity, the dashed line the anisotropic reconstruction and the dotted line the isotropic one. (a) Cross section along the horizontal axis. (b) Cross section along the 45° diagonal.

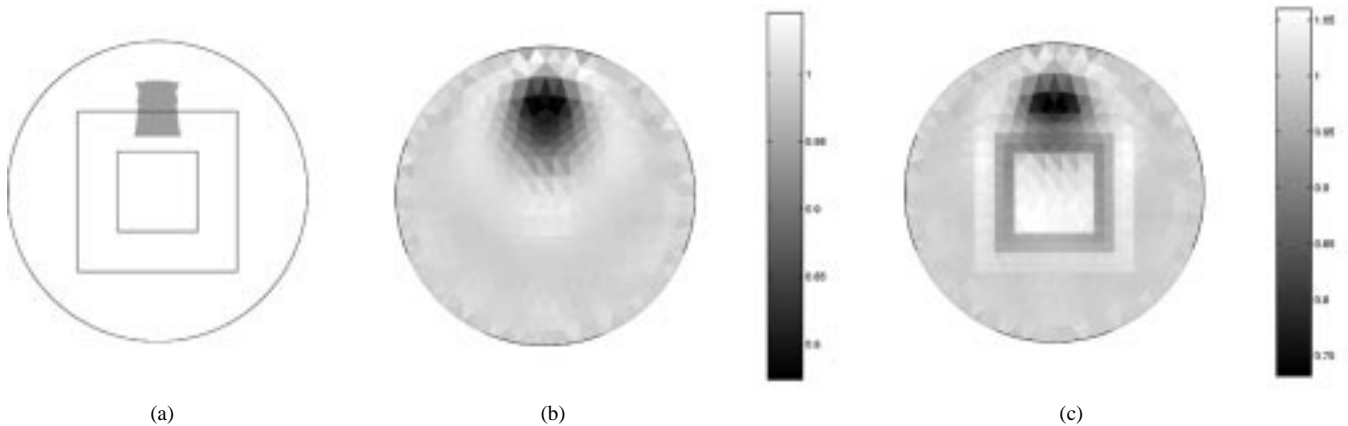


Fig. 7. Inclusion violating the priors. (a) A rectangular inclusion crosses the region Ω_{change} , the prior assumptions are violated, the lateral borders of the inclusion are orthogonal to the expected direction. (b) Isotropic reconstruction of the conductivity. (c) Anisotropic reconstruction of the same conductivity.

IX. GSVD ANALYSIS OF THE RESULTS

GSVD analysis allows study of the problem (3) in the generic case where L is a full rectangular matrix, rather than the more restrictive case of a diagonal matrix allowed by the SVD [16].

The generalized decomposition can be applied, therefore, to the Gaussian filter. Again, the linearization of (3) should be considered

$$\delta \mathbf{s}_{\text{rec}} = \operatorname{argmin} \|J\delta \mathbf{s} - \delta \mathbf{z}\|^2 + \alpha^2 \|L\delta \mathbf{s}\|^2. \quad (28)$$

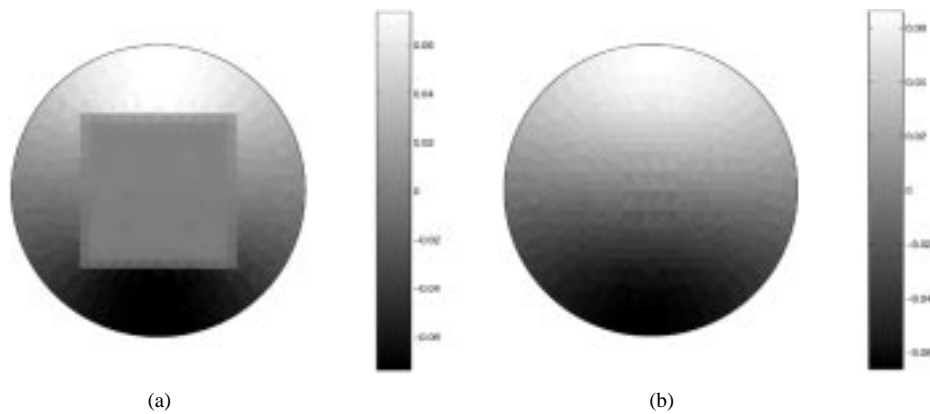


Fig. 8. (a) Second SV calculated with the Gaussian isotropic matrix L . (b) Second SV in the Gaussian anisotropic case.

The matrices $J \in \mathbb{R}^{m \times n}$ and $L \in \mathbb{R}^{p \times n}$ (where p is the number of “regularization constraints,” $p = n$ in the Gaussian case) are then decomposed as

$$\begin{pmatrix} J \\ L \end{pmatrix} = \begin{pmatrix} U & 0 \\ 0 & V \end{pmatrix} \begin{pmatrix} \Lambda & 0 \\ 0 & I_{n-p} \\ M & 0 \end{pmatrix} X^{-1} \quad (29)$$

where $r = \text{rank}(L)$, $U \in \mathbb{R}^{m \times n}$, $V \in \mathbb{R}^{p \times p}$ and $X \in \mathbb{R}^{n \times n}$. The matrices U and V are orthonormal and X nonsingular, Λ and M are diagonal matrices $\in \mathbb{R}^{p \times p}$, $\Lambda = \text{diag}(\lambda_1, \dots, \lambda_p)$ and $M = \text{diag}(\mu_1, \dots, \mu_p)$ with

$$1 \geq \lambda_1 \geq \dots \geq \lambda_r \geq 0, \quad 0 \leq \mu_1 \leq \dots \leq \mu_r \leq 1 \quad (30)$$

and

$$\lambda_i^2 + \mu_i^2 = 1, \quad i = 1, \dots, p. \quad (31)$$

The generalized singular values are defined as $\gamma_i = \lambda_i / \mu_i$ for $i = 1 \dots r$, they appear in nonincreasing order

$$\gamma_1 \geq \gamma_2 \geq \dots \geq \gamma_{r-1} \geq \gamma_r > 0. \quad (32)$$

Using this decomposition, the regularized solutions to the linearized problem (28) can be expressed as

$$\delta \mathbf{s}_{\text{rec}} = \sum_{i=1}^r \frac{\gamma_i^2}{\gamma_i^2 + \alpha^2} \frac{(\mathbf{u}_i^T \delta \mathbf{z})}{\lambda_i} \mathbf{x}_i + \sum_{i=r+1}^n (\mathbf{u}_i^T \delta \mathbf{z}) \mathbf{x}_i. \quad (33)$$

Similar conclusions can be drawn from (33) to those from the SVD analysis. The generalized singular values λ_i show the ill posedness of the problem by rapidly decaying to zero for increasing i . The term $\gamma_i^2 / (\gamma_i^2 + \alpha^2)$ should, therefore, tend to zero with sufficient rapidity to prevent the first term at the right hand side of (33) from diverging. The matrix pair (J, L) is, therefore, understood to regularize the inversion in a similar fashion to (J, I) : by damping the content of the SVs for which the corresponding singular values are too small.

When anisotropic filtering is adopted, we have found interesting changes in the structure that the SVs assume. Typically, the SVs associated with bigger singular values are smooth; they have components only in the lower part of the spectrum of spa-

tial frequencies and do not present discontinuities. The GSVD analysis of the pair (J, L) revealed that with the anisotropic Gaussian filter the structure of the SVs changes.

Fig. 8(a) illustrates the second SV for the isotropic Gaussian filter, which is a vertical gradient as usually happens. The corresponding vector for the anisotropic Gaussian filter is shown in Fig. 8(b). The central region of the image presents a sudden variation corresponding to the area delimited by β_2 . Fig. 9 shows the 14th, 42nd, 108th, and 131st SVs for the anisotropic case. The structural prior information appears to having been embedded in the SVs, modifying the smooth structure that one would expect otherwise. Some of the vectors \mathbf{x}_i decouple the information relative to the inclusion from the background by spanning only particular regions of the image. The nonsmooth properties of the lower SVs allow the reconstruction to describe more easily inclusions matching the prior information, as the spectral analysis explains in more detail.

X. SPECTRAL ANALYSIS

As with the SVD decomposition, it is possible to express a given conductivity distribution \mathbf{s} as a linear combination of the SVs \mathbf{x}_i

$$\mathbf{s} = \sum_{i=1}^n w_i \mathbf{x}_i. \quad (34)$$

The w_i are said to be the spectral coefficients of \mathbf{s} . The actual calculation of the coefficients differs from the standard SVD case in that \mathbf{x}_i are not orthogonal but just linearly independent. The first r spectral coefficients w_i can be calculated as

$$w_i = \langle \mathbf{s}, \mathbf{x}_i \rangle_L \quad i = 1, \dots, r \quad (35)$$

since the vectors \mathbf{x}_i are $L^T L$ orthogonal for $i = 1, \dots, r$, and $\langle \mathbf{x}_i, \mathbf{x}_j \rangle_L = 0$ for $i = 1 \dots r, j = r + 1 \dots n$.

The remaining coefficients can be calculated as

$$w_i = \langle \mathbf{s}, \mathbf{x}_i \rangle_J \quad i = r + 1, \dots, n \quad (36)$$

since the last $n - r$ columns of X are $J^T J$ orthogonal and $\langle \mathbf{x}_i, \mathbf{x}_j \rangle_J = 0$ for $i = 1 \dots r, j = r + 1 \dots n$.

Traditionally, the lower SVs are smooth and the higher ones are oscillatory. Smooth conductivity distributions will, there-

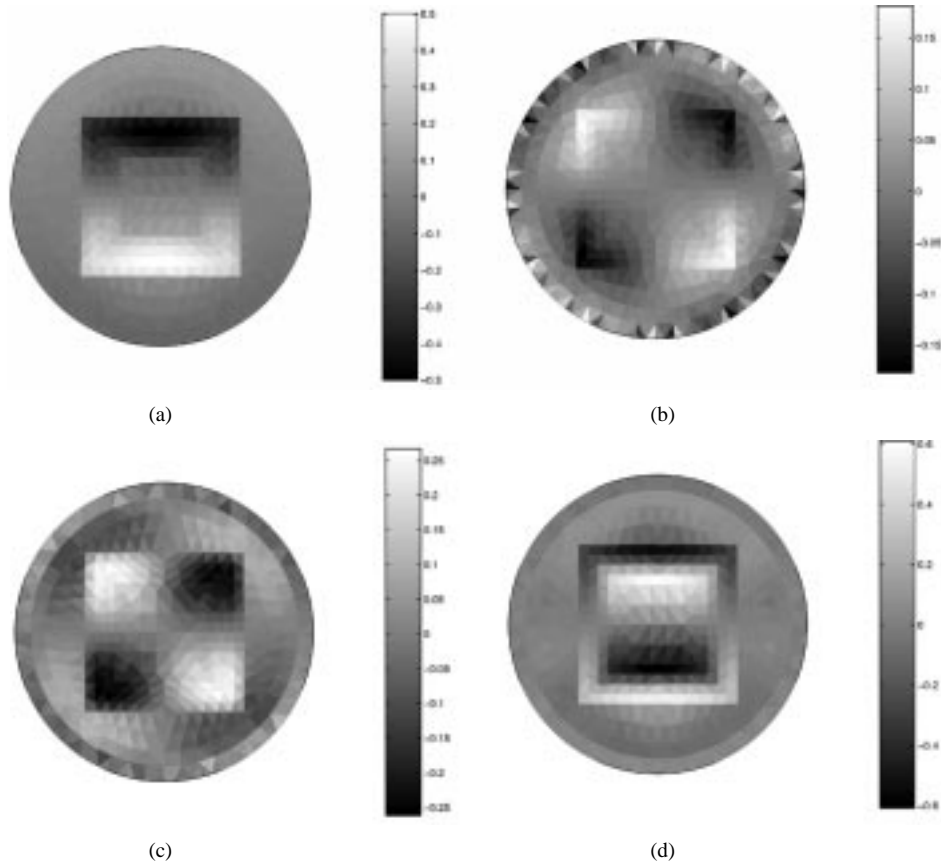


Fig. 9. Generalized SVs calculated with the Gaussian anisotropic matrix L . (a) 14th, (b) 42nd, (c) 108th and (d) 131st.

fore, have components in the lower part of the spectrum and *vice versa*. In this sense, the decomposition (34) is similar to a Fourier analysis of \mathbf{s} .

As introduced earlier, the regularization dampens the contribution of the higher SVs in the image. For a given conductivity distribution \mathbf{s} , the higher the spectral content, the more the reconstructed image will suffer from the dampening. Thus, an image with sharp changes, having significant components in the higher part of the spectrum, will be heavily smoothed. However, when anisotropic filtering is used, the lower SVs are able to span certain sharp transitions, shifting the corresponding components downwards in the spectrum. These conductivity patterns will, therefore, survive the smoothing effect of the regularization.

The spectral shifting property was verified by expanding the test conductivity of Fig. 5(a) in its spectral coefficients, using the SVs derived both from the isotropic and anisotropic filters. The SVs span the conductivity space of the mesh used for the inverse calculations. The test conductivity, defined on a finer mesh, was, therefore, projected onto this mesh. The distribution of the spectral energy was compared by truncating the two expansions at an index k for which

$$\frac{\left\| \sum_{i=1}^k w_i \mathbf{x}_i - \mathbf{s} \right\|}{\|\mathbf{s}\|} < 0.04. \quad (37)$$

The results are shown in the first row of Table I labeled \mathbf{s}_1 . The lower 273 SVs are needed to describe the conductivity \mathbf{s}_1 within 4% error, if isotropic filtering is used. The same conduc-

TABLE I
NUMBER OF SINGULAR VECTORS REQUIRED TO DESCRIBE A TEST
CONDUCTIVITY WITHIN 0.04 ERROR

	iso \mathbf{x}_i	aniso \mathbf{x}_i
\mathbf{s}_1	273	11
\mathbf{s}_2	38	64

tivity is spanned within the same error by the lower 11 SVs in the anisotropic case. The nonsmooth nature of the SVs deriving from the anisotropic filter can, thus, describe a sharp conductivity profile with a smaller spectral content, resulting in less smoothing from the regularization as shown by the reconstructions. The conductivity \mathbf{s}_1 matches the prior information used for setting up the matrix L and for calculating the corresponding SVs. For this reason, the sharp changes in \mathbf{s}_1 are spanned by the lower SVs.

The same experiment was repeated for the test conductivity of Fig. 7(a); the results are reported in the second row of Table I, labeled \mathbf{s}_2 . In this case, the situation differs, 64 SVs are needed to span the image within the 4% error in the anisotropic case, versus 38 for the isotropic regularization. The conductivity \mathbf{s}_2 does not match the prior information, it isn't spanned by the lower SVs, resulting in a slightly worse spectral distribution.

XI. CONCLUSION

In this paper, a method is proposed for dealing with the reconstruction of conductivity images with sharp variations, as encountered in situations of medical interest. The approach is to

enhance the reconstructions by incorporating the prior structural information into the regularization. This is achieved by using Gaussian anisotropic filters, which relax the smoothness in the direction of the expected changes. The effectiveness of the approach has been positively compared with the use of isotropic filters by means of simulations. The simulations show that the sharpness and quantitative estimation of the conductivity are enhanced when the experiment matches the prior information. On the other hand, with a careful selection of the regularization parameters, the algorithm was able to detect a contrast that violated the prior assumptions.

In our view, this paper addresses three different aspects of anisotropic regularization: the introduction of anisotropic Gaussian smoothing, a method for the calculation of the regularization filter and a GSVD analysis of the regularized problem. The first and the last contribution are of general validity. We believe the method we propose for the calculation of L to be best suited for objects with a relatively simple contour, and of reasonably large dimensions compared with the mesh size.

REFERENCES

- [1] M. Cheney, D. Isaacson, J. C. Newell, S. Simake, and J. Goble, "NOSER: An algorithm for solving the inverse conductivity problem," *Int. J. Imag. Syst. Technol.*, vol. 2, pp. 66–75, 1990.
- [2] P. Hua, J. G. Webster, and W. J. Tompkins, "A regularised electrical impedance tomography reconstruction algorithm," *Clin. Phys. Physiol. Meas.*, vol. 9, pp. A137–141, 1988.
- [3] D. C. Dobson and F. Santosa, "An image enhancement technique for electrical impedance tomography," *Inverse Prob.*, vol. 10, pp. 317–334, 1994.
- [4] A. Borsic, C. N. McLeod, and W. R. B. Lionheart, "Total variation regularization in EIT reconstruction," presented at the 2nd World Congr. Industrial Process Tomography, Hannover, Germany, 2001.
- [5] E. J. Woo, P. Hua, J. G. Webster, and W. J. Tompkins, "Measuring lung resistivity using electrical impedance tomography," *IEEE Trans. Biomed. Eng.*, vol. 39, pp. 756–760, July 1992.
- [6] M. Glidewell and K. T. Ng, "Anatomically constrained electrical impedance tomography for anisotropic bodies via a twostep approach," *IEEE Trans. Med. Imag.*, vol. 14, pp. 498–503, Sept. 1995.
- [7] B. M. Eyuboglu, T. C. Pilkington, and P. D. Wolf, "Estimation of tissue resistivities from multiple electrode impedance measurements," *Phys. Med. Biol.*, vol. 39, pp. 1–17, 1994.
- [8] M. Vauhkonen, J. P. Kaipio, E. Somersalo, and P. A. Karjalainen, "Electrical impedance tomography with basis constraints," *Inverse Prob.*, vol. 13, no. 2, pp. 523–530, 1997.
- [9] M. Vauhkonen, D. Vadasz, J. P. Kaipio, E. Somersalo, and P. A. Karjalainen, "Tikhonov regularization and prior information in electrical impedance tomography," *IEEE Trans. Med. Imag.*, vol. 17, pp. 285–293, Apr. 1998.
- [10] J. P. Kaipio, V. Kolehmainen, M. Vauhkonen, and E. Somersalo, "Construction of nonstandard smoothness priors," *Inverse Prob.*, vol. 15, pp. 713–729, 1999.
- [11] A. Tarantola, *Inverse Problem Theory: Methods for Data Fitting and Model Parameter Estimation*. Amsterdam, The Netherlands: Elsevier, 1987.
- [12] A. Adler and R. Guardo, "Electrical impedance tomography: Regularized imaging and contrast detection," *IEEE Trans. Med. Imag.*, vol. 15, pp. 170–179, Apr. 1996.
- [13] E. Somersalo, M. Cheney, and D. Isaacson, "Existence and uniqueness for electrode models for electric current computed tomography," *SIAM J. Appl. Math.*, vol. 52, pp. 1023–1040, 1992.
- [14] Q. S. Zhu, C. N. McLeod, C. W. Denyer, F. J. Lidgley, and W. R. B. Lionheart, "Development of a real-time adaptive current tomograph," *Physiol. Meas.*, vol. 15, pp. A37–A43, 1994.
- [15] B. H. Brown and A. D. Seagar, "Applied potential tomography—Data collection problems," presented at the Inst. Elect. Eng. Int. Conf. Electric and Magnetic Fields in Medicine and Biology, London, U.K., 1985.
- [16] M. Hanke and P. C. Hansen, "Regularization methods for largescale problems," *Surv. Math. Ind.*, vol. 3, pp. 253–315, 1993.